EARTH SCIENCES
RESEARCH JOURNAL
Earth Sci. Res. J. Vol. 29, No. 3 (September, 2025): 275 - 286

UNIVERSIDAD NACIONAL DE COLOMBIA

GEOLOGY

Early Paleoproterozoic continental crust magmatism in the Xueye area, Western Shandong, China: Evidence from U-Pb age and trace element geochemistry of zircon

Wei Tu
School of Geology, Gansu Vocational University of Industry Technology, China

ABSTRACT

The basement of North China Craton (NCC) is a research hotspot in the field of Precambrian geology, as it contains a great deal of information about the formation and evolution of continental lithosphere. In this paper, LA-ICP-MS zircon U-Pb dating and trace element analysis has been carried out on a monzogranite sample from the basement of the Xueye area in Western Shandong, North China. Although no concordia age can be obtained from the $^{206}Pb/^{238}U$ and $^{207}Pb/^{235}U$ data of the zircon grains, these data are distributed along a discordant line, the upper intersection of which gives the formation age of the sample (2356Ma). The concentrations of some trace elements, such as U, Yb, Y, Hf, Th and P, in the zircon grains strongly indicate that the sample is a product of continental crust magmatism. Besides, the relative less extent of Eu anomalies as well as the high concentrations of Th and Pb of the zircon grains indicate that the sample does not belong to anorogenic granitoid. Therefore, the monzogranite is orogenic and its formation may be related to continent-continent or ocean-continent collision. As a result, it can be inferred that a rigid continental plate had been formed by early Paleoproterozoic. Zircon grains in this sample have experienced different extent of alteration since their formation. Most of the zircon grains that have been analyzed have experienced serious alteration, which indicates that there has been intense hydrothermal activity in this area since early Paleoproterozoic.

Keywords: zircon; U-Pb age; trace elements; early Paleoproterozoic; continental crust.

Magmatismo de la corteza continental del Paleoproterozoico temprano en el área de Xueye, oeste de Shandong, China: evidencia de la datación U-Pb y geoquímica de elementos traza del circón

RESUMEN

El basamento del Cratón del Norte de China (NCC) es un foco de investigación en el campo de la geología precámbrica, ya que contiene abundante información sobre la formación y evolución de la litosfera continental. En este trabajo se realizó la datación U-Pb de circón LA-ICP-MS y el análisis de elementos traza en una muestra de monzogranito del basamento del área de Xueye, en el oeste de Shandong, norte de China. Aunque no se puede obtener una edad certera a partir de los datos de $^{206}Pb/^{238}U$ y $^{207}Pb/^{235}U$ de los granos de circón, estos datos se distribuyen a lo largo de una línea discordante, cuya intersección superior proporciona la edad de formación de la muestra (2356Ma). Las concentraciones de algunos elementos traza, como U, Yb, Y, Hf, Th y P, en los granos de circón indican firmemente que la muestra es producto del magmatismo de la corteza continental. Además, la relativa menor extensión de las anomalías de Eu, así como las altas concentraciones de Th y Pb de los granos de circón, indican que la muestra no pertenece a un granitoide anorogénico. Por lo tanto, el monzogranito es orogénico y su formación puede estar relacionada con la colisión continente-continente u océano-continente. Como resultado, se puede inferir que una placa continental rígida se había formado en el Paleoproterozoico temprano. La mayoría de los granos de circón que se han analizado han experimentado una alteración grave, lo que indica que ha habido una intensa actividad hidrotermal en esta área desde el Paleoproterozoico temprano.

Palabras clave: circón; datación U-Pb; elementos traza; Paleoproterozoico temprano; corteza continental.

Record
Manuscript received: 10/05/2023
Accepted for publication: 10/10/2025

How to cite this item:
Tu, W. (2025). Early Paleoproterozoic continental crust magmatism in the Xueye area, Western Shandong, China: Evidence from U-Pb age and trace element geochemistry of zircon. *Earth Sciences Research Journal, 29*(3), 275-286. https://doi.org/10.15446/esrj.v29n3.108296

ISSN 1794-6190 e-ISSN 2339-3459
https://doi.org/10.15446/esrj.v29n3.108296

1. Introduction

The composition, ages, material sources and evolution processes of craton basements are research hotspots in the field of earth science. Detailed research on these issues is conducive to the understanding of the early evolutionary history of the earth. The basement of North China Craton (NCC), which was formed by the amalgamation of several small continental blocks (Zhao, 2009), has a very large outcrop area and has attracted much attention. Western Shandong is a typical region for the outcrops of the Precambrian basement of NCC (Wan et al., 2012) and is an ideal base for the research of the Precambrian history of NCC. There are a great quantity of igneous rocks or metamorphic igneous rocks in the Precambrian basement of Western Shandong (Wang et al., 2008). The above-mentioned rocks have attracted wide attention of geologists because they contain important information about the formation and evolution of the continental lithosphere of this region.

Similar to cratons from other regions of the world, the formation of NCC also includes formation of continental cores (Liu et al., 2024), vast growth of continental crust, collision of small continental plates and cratonization (Zhai and Santosh, 2011; Zhai, 2019; Sun et al., 2021). However, for NCC, there are still disagreements on the time of each stage. Some scholars believe that the peak time of continental crust growth is about 2500Ma and the time of cratonization is about 2300Ma (Zhai and Santosh, 2013; Zhao et al., 2016). While other scholars proposed that cratonization of NCC mainly occurred at about 1850Ma (Kusky and Li, 2003; Peng et al., 2014). However, related research achievements are mainly about Archean magmatism (e.g., Ma et al., 2020; Shan et al., 2021; Wang et al., 2022; Yang et al., 2022), and there are relatively few achievements which are related to Proterozoic magmatism (Wang, 1990; Cao et al., 2017). As a result, it is necessary to improve the research on Proterozoic igneous rocks or metamorphic igneous rocks of this region, which is of great significance for a more complete understanding of the formation and evolution of the Precambrian basement of this region and even that of the whole NCC.

Besides, whole rock geochemistry has been widely used as evidence for the formation and evolution of NCC (e.g., Diwu et al., 2011; Dora et al., 2021), while the components of single minerals have been rarely used. Compared to whole rocks, single minerals have more stable structure and composition. As a result, the geochemical data of single minerals have better comparability and higher sensitivity. With rapid development and popularization of microbeam analysis techniques (e.g., LA-ICP-MS), the costs of the chemical analysis of single minerals have been greatly reduced and the precision has been greatly elevated, which provides favorable conditions for genetic mineralogy research related to chemical composition. Zircon is a common accessory mineral in various kinds of rocks. They can retain some age and chemical information after experiencing multiple episodes of geological events (Grimes et al., 2007). As a result, their isotope and trace element components are of great value for the understanding of the genesis. Besides, zircon is frequently used in isotope dating. A great deal of research has been done and abundant achievements have been accumulated on the relationship between the trace element composition and the genesis of zircon (Grimes et al., 2007). There are abundant zircon grains in igneous rocks, especially acid intrusive rocks. Besides, trace element composition of igneous zircon is very sensitive to source rock types and crystallizing environments (Belousova et al., 2002). Therefore, detailed research on zircon grains from acid intrusive rocks is conducive to the understanding of the origin, evolution, and tectonic background of the magma. In this paper, zircon grains of a monzogranite sample from the basement of NCC have been taken as the research object, U-Pb dating and trace element analysis have been carried out in order to provide more information about the formation, especially the cratonization of NCC.

2. Geological background, sampling and petrographic characteristics

The region of Western Shandong, which is also called Western Shandong Continental Plate, is a relatively stable block located in the west of Shandong Province (Geng et al., 2014). To the east, west and south, Western Shandong Continental Plate is connected to three other continental plates (Bohai Continental Plate, Hebei-Liaoning Continental Plate and Henan-Anhui Continental Plate) by faults, and its northern part is covered by Bohai Sea (Fig. 1) (Geng et al., 2014). Western Shandong Continental Plate has a binary structure which is typical for a platform (Geng et al., 2014). The Precambrian basement of Western Shandong Continental Plate is widely exposed, and its Phanerozoic sedimentary cover lies unconformably upon the Precambrian basement (Geng et al., 2014).

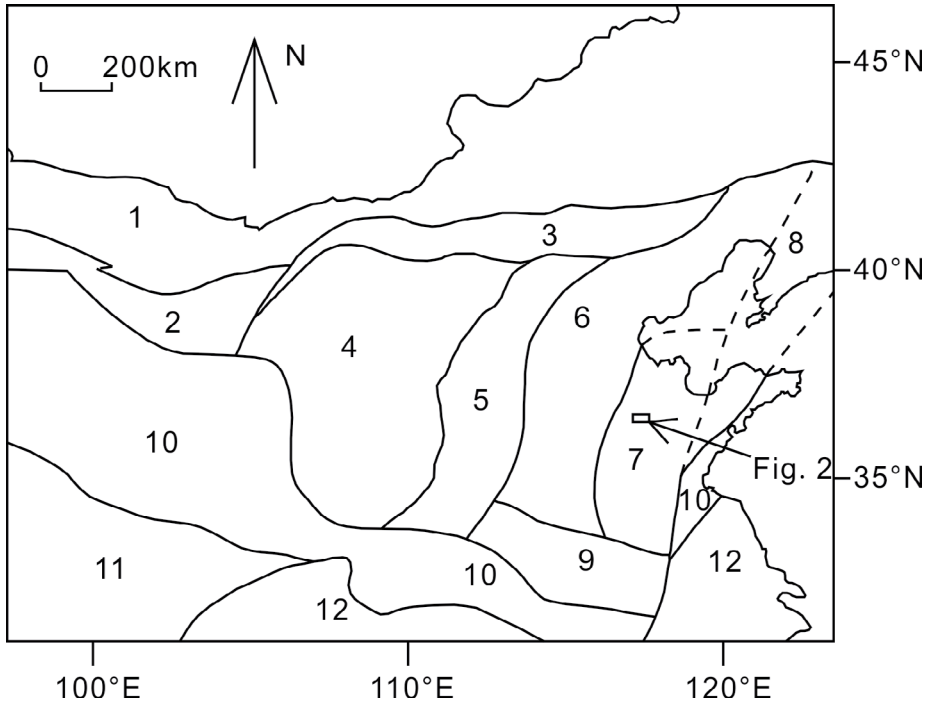

Figure 1. The tectonic location of Western Shandong Continental Plate (1-Tianshan-Xing'an-Mongolian Orogenic System, 2-Tarim Continental Plate Zone, 3-Yinshan-Northern Hebei Continental Plate, 4-Ordos Continental Plate, 5-Wutai-Taihang Continental Plate, 6-Hebei-Liaoning Continental Plate, 7-Western Shandong Continental Plate, 8-Bohai Continental Plate, 9-Henan-Anhui Continental Plate, 10-Qinling-Qilianshan-Kunlunshan Orogenic System, 11-Tibet-Sanjiang Orogenic System, 12-Yangtze Continental Plate Zone, North China Continental Plate Zone includes 3, 4, 5, 6, 7, 8 and 9, after Geng et al., 2014).

The monzogranite sample in this study (SDTS-1) was collected beside No. 327 Provincial Road and near Lijiazhuang Village, Laiwu District, Jinan City. The detailed sampling location is in Figure 2. There is a large area of Paleoproterozoic intrusive or metamorphic intrusive rocks around the sampling location. To the west and not far from the sampling location, there are a large area of Neoarchean intrusive rocks or metamorphic intrusive rocks, while to the north and not far from the sampling location, there are a large area of Paleozoic strata (Fig. 2).

The main minerals of the monzogranite sample are quartz (Fig. 3a, Fig. 3b), alkaline feldspar (Fig. 3a) and plagioclase (Fig. 3b), the proportions of which are 40%, 30%, 25%, respectively. Plagioclase has been obviously altered. This sample is of holocrystalline texture, hypidiomorphic-granular texture and inequigranular texture, besides skeletal texture, myrmetic texture (Fig. 3c) and poikilitic texture (Fig. 3d) can also be seen in this sample, which reflects the complexity of the evolution and crystallization processes of magma (Jia and Huang, 1994). In addition, this sample has a large quantity of fluid inclusions (Fig. 3e and Fig. 3f), most of which are distributed along fractures, indicating that it has been greatly influenced by hydrothermal activity after its formation.

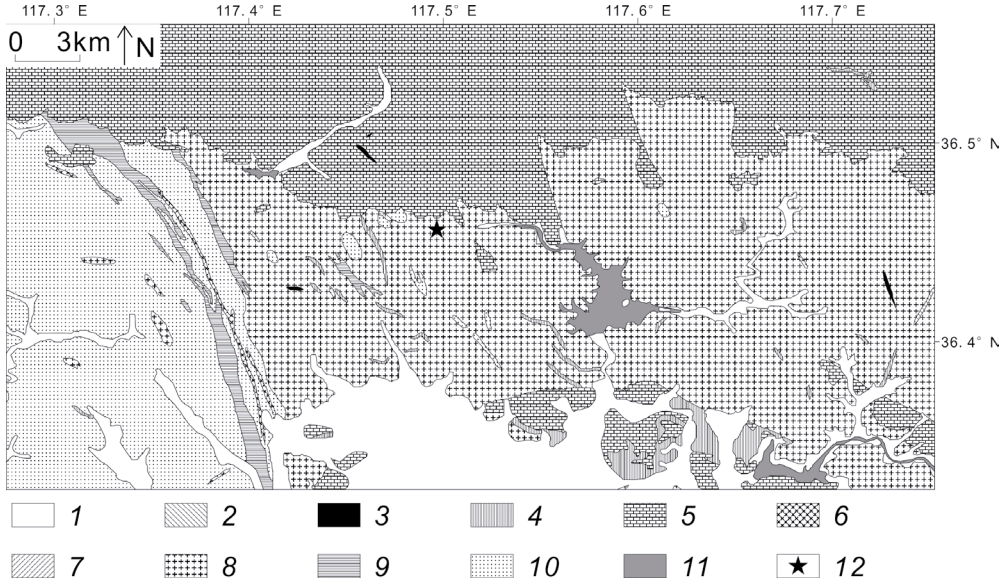

Figure 2. Geological map of the Xueye area of Western Shandong Continental Plate with the location of the monzogranite sample in this study (1-Quaternary, 2-iron vein, 3-early Cretaceous quartz veins, 4-early Cretaceous intrusive rock or metamorphic intrusive rock, 5-Paleozoic strata, 6-Mesoproterozoic intrusive rock or metamorphic intrusive rock, 7-Paleoproterozoic pegmatite vein, 8- Paleoproterozoic intrusive rock or metamorphic intrusive rock, 9-Neoarchean strata, 10-Neoarchean intrusive rock or metamorphic intrusive rock, 11-unknown geological bodies, 12-sampling location, modified from the 1:250000 geological map series of National Geological Archive of China, the location of this map is as in Fig. 1).

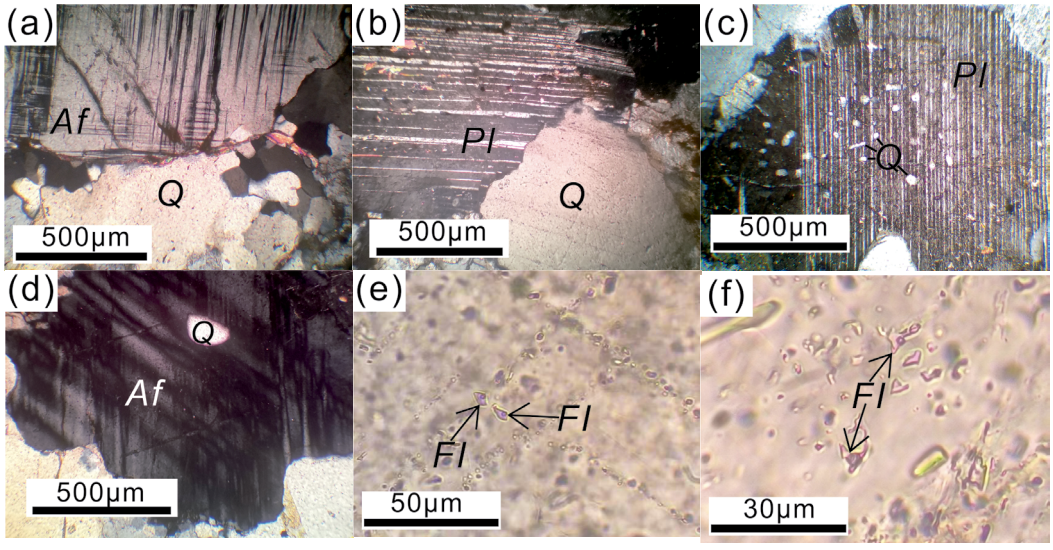

Figure 3. Optical microscopic photos of the monzogranite sample (SDTS-1) (using crossed polarizers). (a) Alkaline feldspar (Af) and quartz (Q). (b) Plagioclase (Pl) and quartz (Q). (c) Quartz (Q) of myrmetic texture in plagioclase (Pl). (d) Quartz (Q) included by alkaline feldspar (Af). (e) Fluid inclusions (FI) in quartz. (f) Fluid inclusions (FI) in alkaline feldspar.

3. Sample processing and analysis methods

The selection of zircon was conducted in the laboratory of Hebei Regional Geological and Mineral Investigation and Research Institute. 524 zircon grains have been selected. These zircon grains were then sent to Wuhan SampleSolution Analytical Technology Co., Ltd. for target preparation, cathodoluminescence photographing, LA-ICP-MS in situ element and isotope analysis and dating. 200 were picked out from the 524 zircon grains for target preparation. The target is 2.54 cm in diameter and its polishing degree met the requirement of the analysis. An Agilent 7900 ICP-MS instrument and a coherent 193 nm excimer laser ablation system (GeoLas HD) were used for LA-ICP-MS in situ element and isotope analysis and dating. The energy, frequency and spot size of the laser were set to 80 mJ, 5 Hz and 32 μm, respectively. The software for data processing is ICPMSDATACAL10.8 (Liu et al., 2008, 2010). The cathodoluminescence photos of the 25 zircon grains analyzed in this study and the sites of the analysis spots are shown in Figure 4. NIST610 and Tanz (Hu et al., 2021) were used as the standard samples for trace element calibration and isotope ratio calibration, respectively. GJ-1, 91500 and Plešovice were used as the standard samples for isotope ratio monitoring. Before and after the analysis of several test samples, Tanz has been analyzed. At the beginning and end of the whole analysis procedure, NIST610 and Tanz have both been analyzed. GJ-1, 91500, and Plešovice were also taken as test samples. The obtained concordia ages for GJ-1, 91500, and Plešovice are 601.5±1.7 Ma (1σ; MSWD=0.076), 1064±5.1 Ma (1σ; MSWD=0.0014) and 335.1±1.2 Ma (1σ; MSWD=0.21), respectively, which are in agreement with the reported or recommended values (GJ-1 = 599.8±1.7 Ma (Liu et al., 2010), 91500 = 1063.8±6.6 Ma (Luan et al., 2019), Plešovice = 337.9±2.8 Ma (Peng et al., 2017)) within the uncertainty ranges.

For LA-ICP-MS analysis, the absolute quantity of the material ablated varies during each run, due to differences in the sample matrix and the related absorption behaviour of the wavelength used for ablation (Liu et al., 2008). An internal standard is generally used to correct the variations, which means that the concentration of at least one element must be known before the analysis (Liu et al., 2008). Because zircon has simple chemical composition, the internal standard can be determined according to the constant stoichiometry (Liu et al., 2008). To conduct quantitative analysis by LA-ICP-MS, the relative sensitivity for each element is usually calibrated using both external calibration and internal standardization (Liu et al., 2008). In this study, NIST610 was chosen as the reference material and Si was chosen as the internal standard element. The concentration of Si in zircon was set to be 15.3%, i.e., the concentration of SiO_2 was set to be 32.7%.

Tanz was chosen as the external standard for U-Pb dating and it would be analyzed before and after the analysis of several test samples (Liu et al., 2010). Time-dependent drifts of U-Th-Pb isotopic ratios were corrected using a linear interpolation method (Liu et al., 2010).

4. Analysis results and discussion

4.1. U-Pb Dating

The results and standard deviations of $^{207}Pb/^{235}U$ and $^{206}Pb/^{238}U$ ratios of the 25 zircon grains are listed in Table 1. $^{207}Pb/^{235}U$ and $^{206}Pb/^{238}U$ ages and their standard deviations are also listed in Table 1. In this study, common lead corrections (^{204}Pb method) have been carried out on part of the data. Because isotopes with the mass number 204 include ^{204}Pb and ^{204}Hg, it is necessary to deduct ^{204}Hg, the quantity of which can be calculated from that of ^{202}Hg. The quantities of ^{206}Pb, ^{207}Pb and ^{208}Pb in common lead can be calculated according to the quantity of ^{204}Pb, lead isotope evolution model of the earth and the estimated age of the sample ($^{206}Pb/^{238}U$ age). Isotope ratios and ages as well as their standard deviations after corrections are listed in Table 2. Common lead corrections have not been carried out on the points No. 5, No. 10, No. 14 and No. 23, because they didn't contain common lead. Fig. 5 and Fig. 6 are $^{206}Pb/^{238}U$-$^{207}Pb/^{235}U$ diagrams before and after common lead corrections, respectively. By comparing the two figures, it can be seen that data before corrections are more dispersive than those after corrections, indicating that the common lead corrections have a good result.

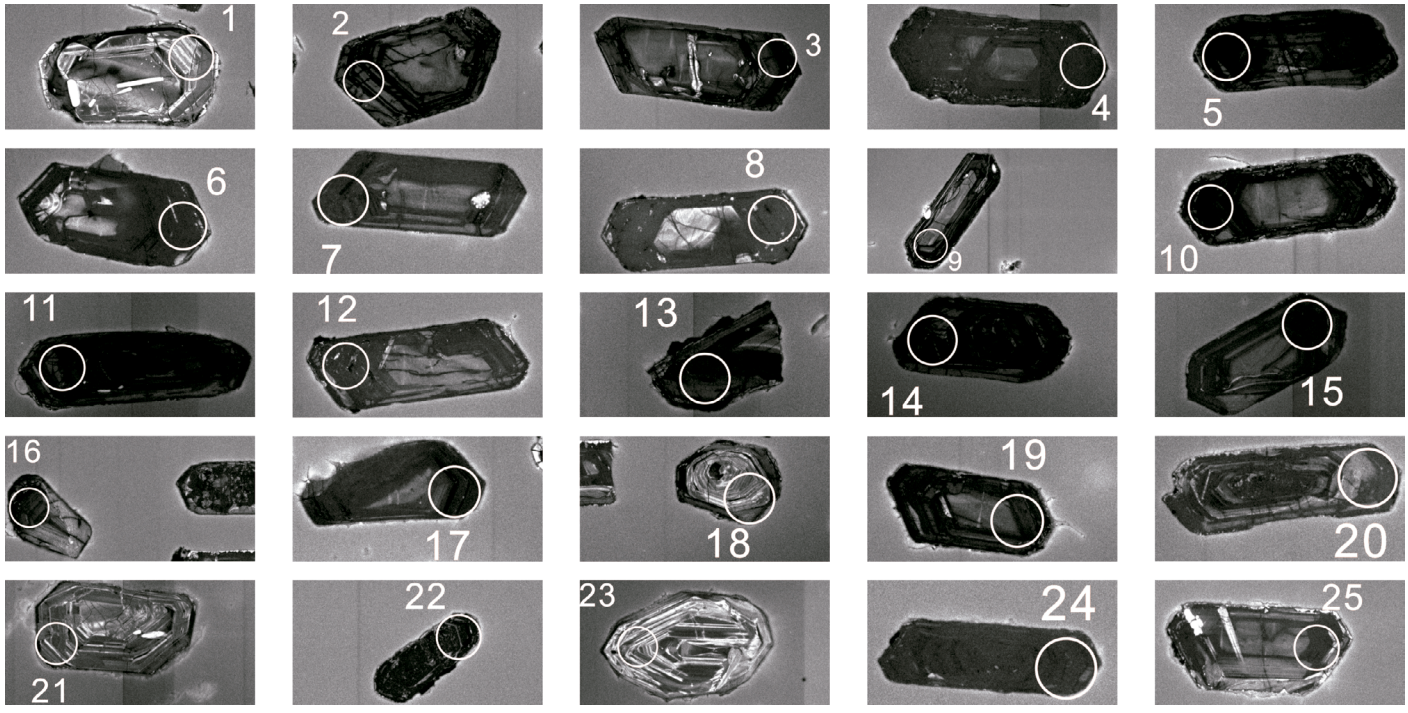

Figure 4. Cathodoluminescence photos of the 25 zircon grains analysed in this study (circles in the photos represent LA-ICP-MS analysis spots, 32 μm across).

Table 1. $^{207}Pb/^{235}U$ and $^{206}Pb/^{238}U$ ratios, ages and their standard deviations before common lead corrections

Analysis point numbers	$^{207}Pb/^{235}U$ ratios	Standard deviations of $^{207}Pb/^{235}U$ ratios	$^{206}Pb/^{238}U$ ratios	Standard deviations of $^{206}Pb/^{238}U$ ratios	$^{207}Pb/^{235}U$ ages (Ma)	Standard deviations of $^{207}Pb/^{235}U$ ages (Ma)	$^{206}Pb/^{238}U$ ages (Ma)	Standard deviations of $^{206}Pb/^{238}U$ ages (Ma)
1	2.8757	0.0382	0.1269	0.0011	1376	10	770	6
2	1.0761	0.0134	0.0344	0.0003	742	7	218	2
3	0.8348	0.0118	0.0323	0.0004	616	7	205	3
4	0.5989	0.0084	0.0220	0.0002	477	5	140	1
5	0.9096	0.0125	0.0146	0.0002	657	7	93.4	1
6	0.4892	0.0085	0.0231	0.0002	404	6	147	1
7	1.2221	0.0168	0.0465	0.0003	811	8	293	2
8	0.9751	0.0140	0.0301	0.0002	691	7	191	1
9	0.7528	0.0125	0.0223	0.0002	570	7	142	1
10	1.1240	0.0137	0.0192	0.0001	765	7	122	1
11	1.0892	0.0183	0.0280	0.0005	748	9	178	3
12	0.8865	0.0129	0.0343	0.0002	644	7	218	2
13	1.0433	0.0312	0.0508	0.0017	726	16	320	10
14	1.2114	0.0194	0.023	0.0002	806	9	146	2
15	0.7917	0.0129	0.0188	0.0002	592	7	120	1
16	1.7211	0.0211	0.0686	0.0006	1016	8	428	4
17	3.6846	0.0789	0.0597	0.0008	1568	17	374	5
18	3.8326	0.0602	0.1739	0.0019	1600	13	1034	10
19	1.3051	0.0168	0.0673	0.0005	848	7	420	3
20	1.0803	0.015	0.049	0.0005	744	7	309	3
21	5.3256	0.1176	0.2505	0.0043	1873	19	1441	22
22	0.6722	0.0109	0.0319	0.0002	522	7	203	1
23	8.4111	0.1965	0.3662	0.0069	2276	21	2011	33
24	1.21	0.0187	0.0326	0.0003	805	9	207	2
25	1.4923	0.0238	0.0451	0.0005	927	10	284	3

Table 2. $^{207}Pb/^{235}U$ and $^{206}Pb/^{238}U$ ratios, ages and their standard deviations after common lead corrections

Analysis point numbers	$^{207}Pb/^{235}U$ ratios	Standard deviations of $^{207}Pb/^{235}U$ ratios	$^{206}Pb/^{238}U$ ratios	Standard deviations of $^{206}Pb/^{238}U$ ratios	$^{207}Pb/^{235}U$ ages (Ma)	Standard deviations of $^{207}Pb/^{235}U$ ages (Ma)	$^{206}Pb/^{238}U$ ages (Ma)	Standard deviations of $^{206}Pb/^{238}U$ ages (Ma)
1	2.3986	0.0352	0.1230	0.0011	1242	11	748	6
2	0.4251	0.0195	0.0289	0.0003	360	14	184	2
3	0.3205	0.0143	0.0280	0.0003	282	11	178	2
4	0.2364	0.0110	0.0189	0.0002	215	9	121	1
5	0.9096	0.0125	0.0146	0.0002	657	7	93.4	1
6	0.2174	0.0118	0.0208	0.0003	200	10	133	2
7	0.5045	0.0223	0.0405	0.0004	415	15	256	2
8	0.3078	0.0215	0.0245	0.0003	272	17	156	2
9	0.2924	0.0150	0.0184	0.0003	260	12	118	2
10	1.1240	0.0137	0.0192	0.0001	765	7	122	1
11	0.3217	0.0264	0.0215	0.0006	283	20	137	4
12	0.3763	0.0163	0.0300	0.0003	324	12	191	2
13	0.6154	0.0126	0.0472	0.0015	487	8	297	9
14	1.2114	0.0194	0.0230	0.0002	806	9	146	2
15	0.1616	0.0218	0.0133	0.0002	152	19	85.4	2
16	0.7215	0.0328	0.0602	0.0005	552	19	377	3
17	0.2018	0.1303	0.0302	0.0013	187	110	192	8
18	3.3986	0.0534	0.1704	0.0018	1504	12	1014	10
19	0.7742	0.0184	0.0628	0.0005	582	11	393	3
20	0.6810	0.0172	0.0456	0.0006	527	10	288	3
21	5.0794	0.1093	0.2486	0.0042	1833	18	1431	22
22	0.4228	0.0133	0.0298	0.0002	358	9	189	1
23	8.4111	0.1965	0.3662	0.0069	2276	21	2011	33
24	0.3129	0.0169	0.0249	0.0003	276	13	158	2
25	0.5526	0.0348	0.0371	0.0007	447	23	235	4

From Figure 6, no concordia age can be obtained from the $^{206}Pb/^{238}U$ and $^{207}Pb/^{235}U$ data of the zircon grains, therefore, a discordant line was drawn (Fig. 7). The ages of the upper and lower intersections of the discordant line and the concordia line are 2356±26[±27] and 100.8±7.0 Ma, respectively. As can be seen from Fig. 6, most zircon grains have experienced severe lead loss, which caused the $^{206}Pb/^{238}U$ and $^{207}Pb/^{235}U$ ages to be much lower than the real age of the sample. Besides, considering all samples in Fig. 6, the ages of the lower intersections are relatively dispersive, indicating that the U-Pb system may have experienced multi-stage evolution or that radiogenic lead may have experienced continuous diffusion loss with time (Li et al., 2004). However, the upper intersections can still reflect the formation time of the sample approximatively (Li et al., 2004). Therefore, the sample was formed in early Paleoproterozoic.

4.2. Zircon Trace Element Analysis

According to in situ microprobe analysis, there are many kinds of trace elements in zircon, of which the ones with high concentrations include Hf, Y, P, U, Th and REE (Hoskin and Schaltegger, 2003). Trace element concentrations as well as some parameters and ratios are listed in Table 3 and Table 4. The intracrystalline distribution of Th and U in igneous zircon is heterogeneous, but the Th/U ratios vary much less (Hoskin and Schaltegger, 2003). The Th/U ratios of igneous zircon are generally greater than 0.5, however, those of metamorphic zircon are generally around 0.01 or even lower (Hoskin and Schaltegger, 2003). The average of the Th/U ratios of the 25 zircon grains in this study is 0.70, indicating that they are typical igneous zircon (Hoskin and Schaltegger, 2003). The partition coefficient of U between zircon and melt is similar to that of Yb, i.e., they have similar compatibility in zircon, which means that the U/Yb ratio of zircon reflects that of the melt in which zircon crystallized (Grimes et al., 2007). The average U/Yb ratios of zircon from different sources are completely different, for example, the average U/Yb ratio of zircon from oceanic gabbro is about 0.18 and that of zircon from continental granitoid is about 1.07 (Grimes et al., 2007). The average U/Yb ratio of the 25 zircon grains in this study is 4.65, which is closer to that of zircon from continental granitoid. Besides, trace elements, such as U, Yb, Hf, Y, Th and P, can be used to discriminate zircons crystallized in continental or oceanic crust settings (Grimes et al., 2007). These zircon grains generally have high U and Th concentrations, but have relatively low Yb and Hf concentrations. In U-Yb diagram, most of the data have been plotted in continental zircon zone (Fig. 8a). In U/Yb-Hf diagram, all of the data have been plotted in continental zircon zone (Fig. 8b). In U/Yb-Y diagram, most of the data have been plotted in or near continental zircon zone, while none of the data have been plotted in oceanic crust zircon zone (Fig. 8c). In Th-Yb diagram, most of the data have been plotted in continental zircon zone (Fig. 8d). In Th/Yb-Hf diagram, most of the data have been plotted in continental zircon zone (Fig. 8e). In Th/Yb-P diagram, most of the data have been plotted in or near continental zircon zone (Fig. 8f). Additionally, trace elements of zircon can also be used to discriminate genetic types of granitoid (Li et al., 2021). These zircon grains have low extent of Eu anomalies but high concentrations of Th and Pb. In Fig. 8g and 8h, most of the data have been plotted in or near S-type or I-type zones, while none of the data have been plotted in A-type zones. The above diagrams indicate that the monzogranite sample is a product of terrigenous magmatic activity and its genetic type is S-type or I-type. In Figs. 8c-8h, some or most of the data are fall outside the representative zones, the main reason for this trend is hydrothermal activity. Some of the zircon grains may have experienced severe hydrothermal alteration. The CI-normalized REE patterns of the zircon grains of the sample are similar to those of orogenic granitoid (I-type and S-type), but quite different from those of anorogenic granitoid (A-type) (Fig. 9). Therefore, this sample belongs to orogenic granitoid and its formation may be related to continent-continent collision or ocean-continent collision.

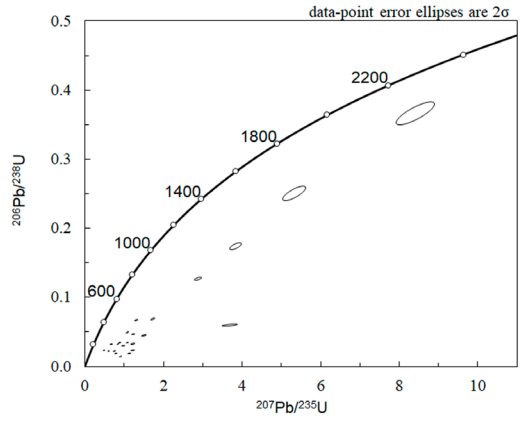

Figure 5. $^{206}Pb/^{238}U$-$^{207}Pb/^{235}U$ diagram of zircon before common lead corrections with the concordia line (the error ellipses correspond to two standard deviations).

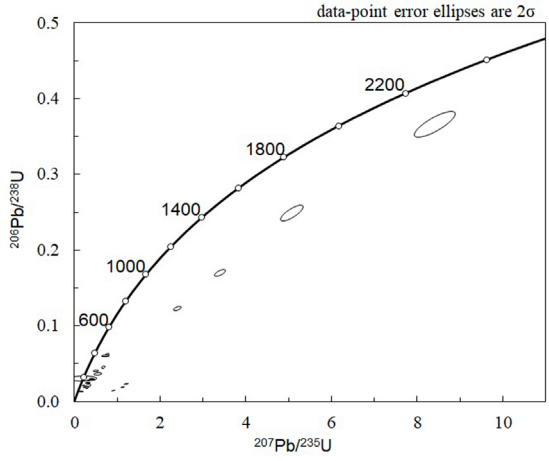

Figure 6. $^{206}Pb/^{238}U$-$^{207}Pb/^{235}U$ diagram of zircon after common lead corrections with the concordia line (the error ellipses correspond to two standard deviations).

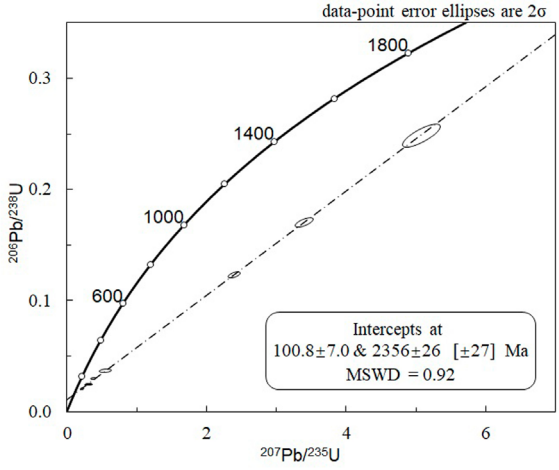

Figure 7. $^{206}Pb/^{238}U$-$^{207}Pb/^{235}U$ diagram of zircon after common lead corrections with the concordia line and a discordant line (the error ellipses correspond to two standard deviations, two ages in the figure are ages for the lower and upper intersections, MSWD stands for mean squared weighted deviation).

Table 3. REE concentrations (ppm) and δEu of zircon

Analysis point numbers	La	Ce	Pr	Nd	Sm	Eu	Gd	Tb	Dy	Ho	Er	Tm	Yb	Lu	ΣREE	$\delta E u^{(a)}$
1	16.3	104	13.0	82.6	67.8	20.1	129	23.1	162	43.4	166	33.2	317	61.4	1238.6	0.66
2	251	833	149	762	477	129	714	157	1068	218	607	92.2	655	93.9	6205.5	0.67
3	229	958	155	939	859	246	1567	336	2180	449	1333	236	1853	284	11623.6	0.65
4	97.2	1015	102	906	1029	140	1203	160	821	163	465	75.6	619	108	6903.9	0.38
5	1149	2205	580	2942	1951	277	3212	810	6086	1428	4431	759	5203	684	31717.7	0.34
6	111	2074	218	1716	896	156	882	139	932	219	711	121	950	153	9276.7	0.54
7	165	1170	167	1043	419	43.7	402	67.5	450	108	363	67.4	555	95.7	5115.3	0.32
8	108	1374	137	1083	616	113	681	121	715	146	443	76.6	632	110	6355.3	0.53
9	461	988	229	1217	895	158	1448	346	2638	604	1995	347	2595	329	14249.0	0.42
10	504	1820	341	1806	1495	284	2904	524	2968	543	1358	193	1353	203	16297.1	0.42
11	195	897	148	1026	1041	245	1444	247	1451	291	786	115	804	118	8807.8	0.61
12	91.4	3414	300	3390	883	149	721	99.0	765	211	830	168	1472	229	12724.3	0.57
13	77.7	637	77.3	436	363	167	674	133	939	208	652	105	770	116	5355.9	1.03
14	796	1386	389	1890	1258	231	1875	346	2081	408	1093	168	1205	165	13292.1	0.46
15	256	1603	179	1252	1121	331	1506	194	980	189	553	91.7	753	119	9126.1	0.78
16	90.9	486	72.6	485	428	86.8	716	114	575	109	307	51.8	418	73.1	4012.9	0.48
17	173	974	150	768	270	87.0	337	64.6	466	118	415	77.7	645	106	4651.0	0.88
18	8.76	101	9.23	63.0	61.7	10.1	103	22.1	156	39.6	142	27.7	258	50.8	1053.2	0.38
19	90.2	969	97.2	492	231	104	327	82.7	685	176	661	130	1085	167	5297.1	1.15
20	183	1262	133	1030	504	76.1	457	57.9	306	67.2	220	44.0	406	78.1	4825.6	0.48
21	5.97	123	11.7	96.6	73.0	8.94	97.1	15.8	103	27.6	103	20.3	187	36.6	909.4	0.32
22	103	802	77.2	595	1204	597	2073	179	891	193	603	104	853	139	8411.6	1.15
23	2.20	12.6	0.63	5.15	5.75	0.90	20.2	5.06	47.0	15.7	65.1	12.3	111	20.7	324.4	0.25
24	42.1	684	54.7	1320	946	219	590	56.2	334	82.4	296	59.4	590	129	5404.1	0.90
25	82.3	1123	87.5	842	492	69.2	519	80.3	468	102	322	55.6	459	79.8	4782.6	0.42

[(a)]Trace element concentrations of CI carbonaceous chondrite used for δEu are from McDonough and Sun, 1995.

Table 4. Concentrations of some other trace elements of zircon (ppm) and some ratios between trace element concentrations of zircon

Analysis point numbers	P	Ti	Y	Nb	Hf	Ta	Pb	Th	U	Th/U	U/Yb	Th/Yb	$(Nb/Pb)_N$[(a)]
1	1313	28.8	1349	6.78	9334	1.73	192.8	524	1148	0.46	3.62	1.65	0.36
2	2882	146	5905	38.6	11036	5.75	253	1651	4779	0.35	7.30	2.52	1.57
3	3310	240	12261	142	19275	18.4	217.1	2703	4832	0.56	2.61	1.46	6.71
4	638	281	5038	48.7	10860	8.40	129.5	2440	3732	0.65	6.03	3.94	3.87
5	11151	412	33691	357	14023	15.9	453	39197	12702	3.09	2.44	7.53	8.10
6	788	97.7	6105	47.1	13870	16.9	127.1	1801	3784	0.48	3.98	1.90	3.81
7	442	77.7	2916	26.2	9806	9.24	184.0	1989	2509	0.79	4.52	3.58	1.47
8	428	86.7	3972	22.4	10600	10.1	136.6	1752	2643	0.66	4.18	2.77	1.69
9	4263	142	14203	130	7897	3.76	253	5240	6358	0.82	2.45	2.02	5.27
10	2150	278	15517	70.0	13767	17.2	511	3032	11465	0.26	8.47	2.24	1.41
11	1431	228	8188	52.8	9613	6.26	301	1535	5790	0.27	7.20	1.91	1.81
12	1506	15.6	7867	27.0	9950	10.7	108.2	2243	1948	1.15	1.32	1.52	2.57
13	1025	192	5828	49.7	8290	3.20	194.8	998	3286	0.30	4.27	1.30	2.62
14	2010	337	10422	42.3	11208	10.5	407	2427	8597	0.28	7.13	2.01	1.07
15	1254	135	6107	50.6	9662	9.23	282	3194	7529	0.42	10.00	4.24	1.85
16	583	54.2	3016	17.5	8046	4.40	258	2108	2385	0.88	5.71	5.04	0.70
17	832	129	3242	45.4	9773	10.4	469	2130	3105	0.69	4.81	3.30	1.00
18	256	21.4	1113	11.9	9680	10.8	183.3	406	831	0.49	3.22	1.57	0.67
19	1000	131	4578	22.1	7910	4.11	204	4276	1977	2.16	1.82	3.94	1.11
20	343	105	2126	22.9	11667	16.3	134.4	767	2041	0.38	5.03	1.89	1.76
21	235	17.4	836	4.83	8650	1.67	160.7	199	545	0.37	2.91	1.06	0.31
22	901	225	6347	108	11620	12.6	173.2	1615	4047	0.40	4.74	1.89	6.39
23	321	8.08	475	1.68	7786	0.93	180.5	158	423	0.37	3.81	1.42	0.10
24	257	95.7	2734	38.4	15273	24.7	139.9	523	2420	0.22	4.10	0.89	2.83
25	391	113	2972	16.1	8409	8.40	172	2364	2118	1.12	4.61	5.15	0.96

[(a)]Trace element concentrations of CI carbonaceous chondrite used for $(Nb/Pb)_N$ are from McDonough and Sun, 1995.

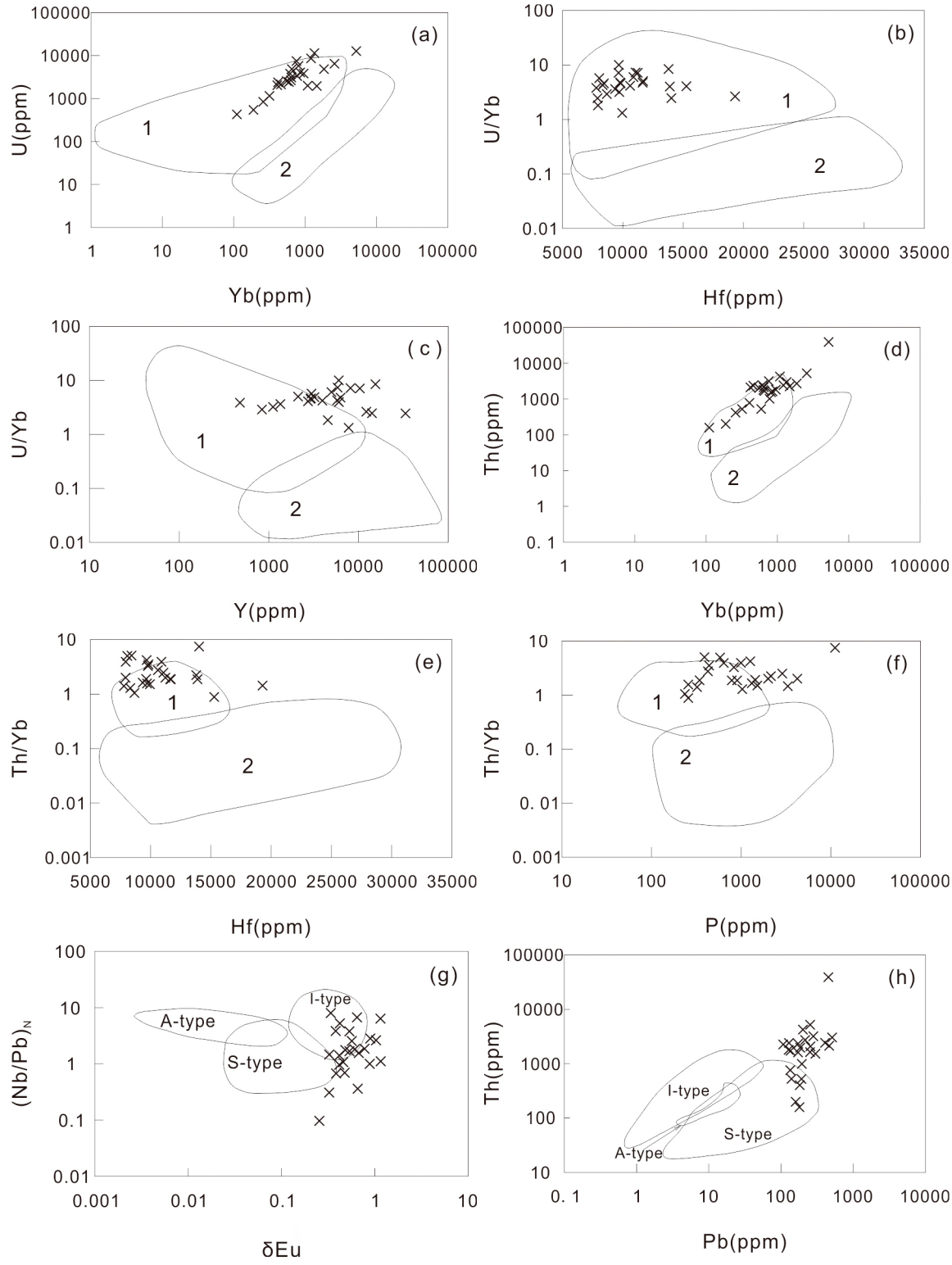

Figure 8. Zircon trace element discrimination diagrams. (a) U-Yb diagram. (b) U/Yb-Hf diagram. (c) U/Yb-Y diagram. (d) Th-Yb diagram. (e) Th/Yb-Hf diagram. (f) Th/Yb-P diagram. (g) $(Nb/Pb)_N$-δEu diagram. (h) Th-Pb diagram. (a), (b), (c), (d), (e) and (f) are according to Grimes et al., 2007. (g) and (h) are according to Li et al., 2021. Trace element concentrations of CI carbonaceous chondrite used for (g) are from McDonough and Sun, 1995. In Figures (a) to (f), 1 means continental crust zircon, 2 means ocean crust zircon.

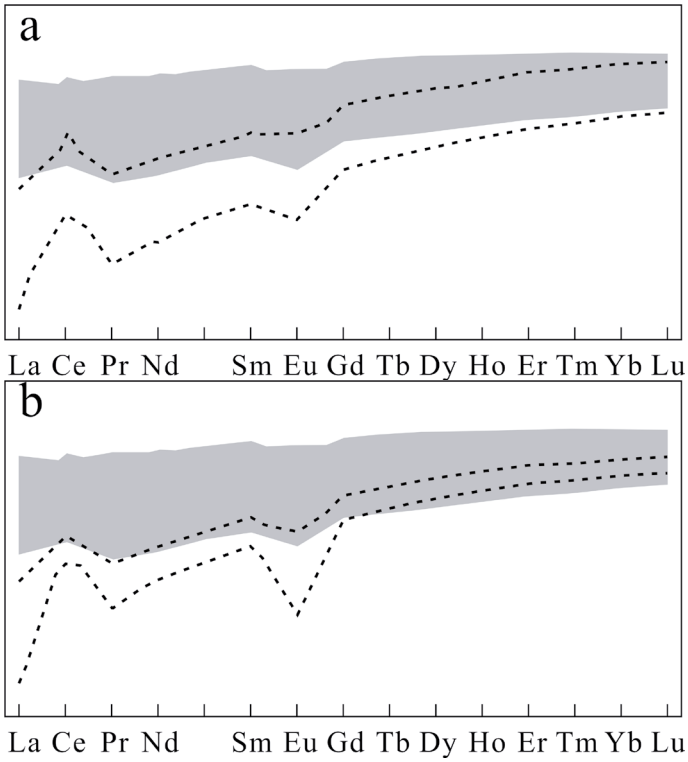

Figure 9. Zircon CI-normalized REE patterns of the sample in this study and samples from well-established continental settings (gray zones: the sample in this study, dashed line in a: continental orogenic granitoid, dashed line in b: continental anorogenic granitoid)

5. Conclusions

U-Pb isotope analysis of zircon from a monzogranite sample from the Xueye area of Western Shandong indicates that the age of the sample is 2356±26[±27] Ma (early Paleoproterozoic). Zircon geochemistry of the sample indicates that it is a product of continental crust magmatic activity, which may be related to continent-continent or ocean-continent collision. Therefore, a rigid continental plate had been formed by early Paleoproterozoic in this region. Zircon grains in this sample have experienced different extent of alteration since their formation. Most of the zircon grains that have been analyzed have experienced serious alteration, which indicates that there has been intense hydrothermal activity in this region since early Paleoproterozoic.

Acknowledgments

The author is grateful to Zheng Liu, laboratory technician of Wuhan SampleSolution Analytical Technology Co., Ltd., for research assistance. This study was supported by a research fund of Huaiyin Institute of Technology (No. Z301B18559).

References

Belousova, E. A., Griffin, W. L., O'Reilly, S. Y., & Fisher, N. I. (2002). Igneous zircon: trace element composition as an indicator of source rock type. *Contributions to Mineralogy and Petrology*, 143, 602-622. https://doi.org/10.1007/s00410-002-0364-7

Cao, G., Shan, W., Yan, K., & Gou, D. (2017). Distribution and property characteristics of intrusive rocks in Mengshan Mountain in Shandong Province. *Shandong Land and Resources,* 33, 1-5.

Diwu, C., Sun, Y., Guo, A., Wang, H. & Liu, X. (2011). Crustal growth in the North China Craton at ~ 2.5 Ga: Evidence from in situ zircon U–Pb ages, Hf isotopes and whole-rock geochemistry of the Dengfeng complex. *Gondwana Research*, 20(1), 149-170. https://doi.org/10.1016/j.gr.2011.01.011

Dora, M. L., Upadhyay, D., Malviya, V. P., Meshram, T., Baswani, S. R., Randive, K., Meshram, R., Suresh, G., Naik, R., & Ranjan, S. (2021). Neoarchaean and Proterozoic crustal growth and reworking in the Western Bastar Craton, Central India: Constraints from zircon, monazite geochronology and whole-rock geochemistry. *Precambrian Research*, 362, 106284. https://doi.org/10.1016/j.precamres.2021.106284

Geng, K., Li, H., Liang, T., Zhuo, C., & Zhang, Y. (2014). Precambrian tectonic evolution of Luxi Landmass. *Shandong Land and Resources*, 30, 1-8.

Grimes, C. B., John, B. E., Kelemen, P. B., Mazdab, F. K., Wooden, J. L., Cheadle, M. J., Hanghøj, K. & Schwartz, J. J. (2007). Trace element chemistry of zircons from oceanic crust: A method for distinguishing detrital zircon provenance. *Geology*, 35, 643-646. https://doi.org/10.1130/G23603A.1

Hoskin, P. W. O. & Schaltegger, U. (2003). The composition of zircon and igneous and metamorphic petrogenesis. *Reviews in Mineralogy and Geochemistry*, 53, 27-62. https://doi.org/10.2113/0530027

Hu, Z., Li, X., Luo, T., Zhang, W., Crowley, J., Li, Q., Ling, X., Yang, C., Li, Y., Feng, L., Xia, X., Zhang, S., Wang, Z., Guo, J., Xu, L., Lin, J., Liu, X., Bao, Z., Liu, Y., Zong, K., Chen, W., & Hu, S. (2021). Tanz zircon megacrysts: a new zircon reference material for the microbeam determination of U-Pb ages and Zr-O isotopes. *Journal of Analytical Atomic Spectrometry,* 36, 2715-2734. https://doi.org/10.1039/D1JA00311A

Jia, B., & Huang, Z. (1994). *A Concise Tutorial on Igneous and Metamorphic Petrology*. China Coal Industry Publishing House, Beijing, China, 227 pp.

Kusky, T. M., & Li, J. (2003). Paleoproterozoic tectonic evolution of the North China Craton. *Journal of Asian Earth Sciences*, 22(4), 383-397. https://doi.org/10.1016/S1367-9120(03)00071-3

Li, J., Huang, H., Liu, Z., Zhang, T., Wang, Q., Fang, S., & Zou, M. (2021). LA-ICP-MS U-Pb ages and trace element compositions of zircon from Indosinian granites in middle Zhuguangshan. *Geotectonica et Metallogenia*, 45, 1216-1232. DOI: 10.16539/j.ddgzyckx.2021.06.007

Li, Z., Lu, Y. & Huang, G. (2004). *Methods and Progress on Radioactive Isotope Geology*. China University of Geosciences Press, Wuhan, China, 276 pp.

Liu, J., Palin, R. M., Mitchell, R. N., Liu, Z., Zhang, J., Li, Z., Cheng, C., & Zhang, H. (2024). Archaean multi-stage magmatic underplating drove formation of continental nuclei in the North China Craton. *Nature Communications*, 15, 6231. https://doi.org/10.1038/s41467-024-50435-5

Liu, Y., Hu, Z., Gao, S., Günther, D., Xu, J., Gao, C., & Chen, H. (2008). In situ analysis of major and trace elements of anhydrous minerals by LA-ICP-MS without applying an internal standard. *Chemical Geology*, 257, 34-43. https://doi.org/10.1016/j.chemgeo.2008.08.004

Liu, Y., Gao, S., Hu, Z., Gao, C., Zong, K., & Wang, D. (2010). Continental and oceanic crust recycling-induced melt-peridotite interactions in the Trans-North China Orogen: U-Pb dating, Hf isotopes and trace elements in zircons from mantle xenoliths. *Journal of Petrology*, 51, 537-571. https://doi.org/10.1093/petrology/egp082

Luan, Y., He, K. & Tan, X. (2019). In situ U-Pb dating and trace element determination of standard zircons by LA-ICP-MS. *Geological Bulletin of China*, 38, 1206-1218.

Ma, M., Wan, Y., Xie, H., Liu, S., Xie, S., Dong, C., Bai, W., Li, Y., & Wang, Y. (2020). Neoarchean mafic magmatism in Qixingtai Area, West Shandong: Formation ages and compositions of meta-gabbros. *Earth Science*, 45, 2610-2628. https://doi.org/10.3799/dqkx.2020.190

McDonough, W. F. & Sun, S. (1995). The composition of the Earth. *Chemical Geology*, 120, 223-253. https://doi.org/10.1016/0009-2541(94)00140-4

Peng, L., Li, Q., Chai, F., Yan, J., & Liu, X. (2017). Single zircon in situ U-Pb age by LA-ICPMS at small beam spot. Journal of Hefei University of Technology (Natural Science), 40, 110-116. DOI: 10.3969/j.issn.1003-5060.2017.01.020

Peng, P., Wang, X., Windley, B. F., Guo, J., Zhai, M., & Li, Y. (2014). Spatial distribution of ~ 1950-1800 Ma metamorphic events in the North China Craton: Implications for tectonic subdivision of the craton. *Lithos*, 202-203, 250-266. https://doi.org/10.1016/j.lithos.2014.05.033

Shan, L., Niu, Y., & Ma, S. (2021). Petrogenesis of the Neoarchean diorite and hornblendite in the Taishan area, western Shandong: Constraints on crustal evolution. *Geological Bulletin of China,* 40, 1149-1177.

Sun, G., Liu, S., Cawood, P. A., Tang, M., van Hunen, J., Gao, L., Hu, Y., & Hu, F. (2021). Thermal state and evolving geodynamic regimes of the Meso- to Neoarchean North China Craton. *Nature Communications*, 12, 3888. https://doi.org/10.1038/s41467-021-24139-z

Wan, Y., Liu, D., Wang, S., Jiao, X., Wang, W., Dong, C., Xie, H., & Ma, M. (2012). Redefinition of Early Precambrian supracrustal rocks and formation age of BIF in western Shandong, North China Craton. *Acta Petrologica Sinica*, 28, 3457-3475.

Wang, S. (1990). The Precambrian intrusive rocks in the west Shandong, China. *Shandong Geology,* 6, 59-81.

Wang, S., Wan, Y., Zhang, C., Yang, E., Song, Z., Wang, L., & Zhang, F. (2008). Major advanced development gained in studying early Cambrian geology in Luxi area. *Shandong Land and Resources,* 24, 10-20.

Wang, Y., Zhou, Q., Zhang, J., & Zhou, G. (2022). Neoarchean crustal accretion in western Shandong Province: Evidence from granite and monzogranite U-Pb chronology, Hf isotope and rock geochemistry. *Journal of Jilin University (Earth Science Edition),* 52, 463-485. DOI: 10.13278/j.cnki.jjuese.20210164

Yang, F., Chen, Y., & Yu, Y. (2022). Genesis and geological significance of late Archean syeno-monzogranite in Western Shandong Province. *Geoscience*, 36, 1155-1172. DOI: 10.19657/j.geoscience.1000-8527.2022.04.18

Zhai, M. (2019). Tectonic evolution of the North China Craton. *Journal of Geomechanics*, 25(5), 722-745. DOI: 10.12090/j.issn.1006-6616.2019.25.05.063

Zhai, M., & Santosh, M. (2011). The early Precambrian odyssey of the North China Craton: A synoptic overview. *Gondwana Research*, 20(1), 6-25. https://doi.org/10.1016/j.gr.2011.02.005

Zhai, M., & Santosh, M. (2013). Metallogeny of the North China Craton: Link with secular changes in the evolving Earth. *Gondwana Research*, 24(1), 275-297. https://doi.org/10.1016/j.gr.2013.02.007

Zhao, G. (2009). Metamorphic evolution of major tectonic units in the basement of the North China Craton: Key issues and discussion. *Acta Petrologica Sinica*, 25, 1772-1792.

Zhao, L., Zhu, X., & Zhai, M. (2016). Major advances in the study of the Precambrian geology and metallogenesis of the North China Craton: A review. *Acta Geologica Sinica (English Edition),* 90(4), 1122-1155. https://doi.org/10.1111/1755-6724.12765